Discover Materials

Research

Reactivity of a plagioclase concentrate from the South African Bushveld Igneous Complex via extractive acid leaching vs. extractive roasting-leaching processes

Sameera Mohamed[1,2] · Elizabet M. van der Merwe[2] · Zakhele H. Nkosi[3] · Wladyslaw Altermann[3,4] · Wiebke Grote[3] · Frédéric J. Doucet[1]

Received: 2 July 2024 / Accepted: 20 September 2024
Published online: 01 October 2024

Abstract
This study compared the reactivity of a plagioclase concentrate subjected to two processes: (1) direct acid leaching and (2) thermochemical treatment with ammonium sulfate followed by leaching. The sample was prepared from coarse-grained pyroxenite rock retrieved from the Bushveld Igneous Complex, South Africa. It contained 78% plagioclase (labradorite), 9% orthopyroxene (enstatite) and 13% quartz. The elements contained in the concentrate were categorized into three groups based on their susceptibility to direct acid extraction after 6 h of leaching. Group 1 consisted of the highly reactive main elements of plagioclase (Al, Ca and Na, with extraction efficiencies of 95%, 89% and 81%, respectively). Group 2 included elements predominantly present in enstatite (Mg and Fe with extraction efficiencies of 41% and 55%, respectively). Group 3 was composed of slowly extractable Si (25%) from mostly plagioclase. Increasing the duration of direct acid leaching to 24 h had no effect on the extraction of Group 1 elements, whereas the extraction of Mg and Fe (Group 2) increased to >60%, and that of Si (Group 3) increased from 25 to 80%. The latter correlated with the nearly complete disappearance of the plagioclase blueprint in the XRD pattern of the residues generated after 24 h of leaching. In contrast, plagioclase had limited reactivity with ammonium sulfate during thermochemical treatment. Direct acid leaching of plagioclase-rich tailings can therefore generate leachates to be used as precursors for the preparation of value-added products, such as silica nanoparticles via a sol–gel route and calcium aluminate nanoparticles via solution combustion.

Keywords Plagioclase · Elemental extraction · Acid leaching · Thermochemical treatment · Ammonium sulfate

1 Introduction

Silicates represent the most abundant group of minerals on Earth and are ubiquitous in mineral and mining wastes. Understanding their chemical reactivity under varying conditions is essential [5] since they are involved in numerous important industrial processes, such as carbon dioxide (CO_2) mineral sequestration [36], vitrified nuclear waste disposal

Supplementary Information The online version contains supplementary material available at https://doi.org/10.1007/s43939-024-00125-2.

✉ Frédéric J. Doucet, fdoucet@geoscience.org.za; Sameera Mohamed, smohamed@geoscience.org.za; Elizabet M. van der Merwe, liezel.vandermerwe@up.ac.za; Zakhele H. Nkosi, zakhele.nkosi@up.ac.za; Wladyslaw Altermann, altermannw@gmail.com; Wiebke Grote, grotewiebke@gmail.com | [1]Council for Geoscience, Private Bag X112, Pretoria 0001, South Africa. [2]Department of Chemistry, University of Pretoria, Lynnwood Road, Pretoria 0002, South Africa. [3]Department of Geology, University of Pretoria, Lynnwood Road, Pretoria 0002, South Africa. [4]Present Address: Freelance Geological Consultant, Pretoria, South Africa.

[14–16], the extraction of strategic metals from silicate-bearing materials (e.g., coal fly ash [11, 45, 50], the treatment of laterite nickel ore [25], platinum group metal (PGM) tailings [33, 35], bauxite residue [4] and the purification of silicate minerals (e.g., talc [8]). Such studies can lead to the large-scale reprocessing and reuse of mineral and mining wastes and can facilitate the development of new materials and novel processing routes [49], they can therefore address issues related to the Green Agenda such as the sustainable use of the world's finite natural mineral resources and the protection of the environment [26].

In South Africa, the reactivity of silicate-bearing PGM tailings from the Bushveld Igneous Complex (BIC) is of particular interest due to their abundance, with the country accounting for 96% of known global reserves of PGM [31], and their perceived CO_2 mineralization potential owing to their Mg-rich mineralogy [10, 48]. These high-tonnage mining waste materials also contain elevated concentrations of Ca, Al, Fe, and Cr and low to moderate amounts of Ti and other valuable elements, depending on their origin [32]. However, their complex mineralogy and associated chemical reactivity remain challenging. For instance, Meyer et al. [28] reported that acid leaching using both strong inorganic (2 M HCl) and organic (oxalic acid, ethylenediaminetetraacetic [EDTA]) acids had limited value for cation extraction from PGM tailings, with only up to 3% Mg, 9% Fe and 30% Ca extracted. More recently, Mohamed et al. [35] examined a promising two-stage process, which consists of a solid−solid thermochemical extraction step (stage one) using ammonium sulfate salt ($(NH_4)_2SO_4$) as a chemical agent, followed by an optimized acid HNO_3 leaching step (stage two). This process yielded promising extraction efficiencies (80% Ca, 60% Al, 35% Fe, 32% Si, 27% Cr and 25% Mg). Additional experiments [34] provided the first hint that the optimal extraction efficiencies achieved using this two-stage process could not be ascribed solely to the effect of the thermochemical step for all major elements. More specifically, (1) most of the Si and Ca were extracted via the acid dissolution step, (2) Al and Mg were extracted at each stage of the process, and (3) the thermochemical step was the main contributor to Cr and Fe extraction. The optimized acid dissolution step, in the absence of the thermochemical step, can be assimilated to a conventional hydrometallurgical process of HNO_3 leaching for elemental recovery from PGM tailings. However, not all inorganic acids were equally effective at extracting Ca and Si from PGM tailings, with HNO_3 [34] being much more effective than HCl [28]. While $(NH_4)_2SO_4$ was more reactive than other ammonium salts (ammonium bisulfate NH_4HSO_4, ammonium chloride NH_4Cl, ammonium nitrate NH_4NO_3) with silicates contained in PGM tailings during thermochemical treatment [33], Ca was nearly equally extracted for all salts, which provided additional evidence that Ca may have been extracted during the acid dissolution step rather than during the thermochemical step. However, Mohamed et al. [33] could not ascertain (1) whether the plagioclase phase, which was thought to be the main Ca-bearing mineral in the tailings, reacted with $(NH_4)_2SO_4$ or other ammonium salts during the thermochemical step or (2) whether the HNO_3 dissolution step on its own, which appeared to be able to extract most of the Ca and probably most of the Al contained in the plagioclase phase, could also destabilize the entire Si network of the plagioclase mineral. Elucidating these questions is of particular importance for the valorization of some South African PGM tailings, which can contain up to 60% plagioclase feldspars in the form of Ca-rich plagioclase. It is also of relevance to the valorization of other mining and industrial residues that contain this mineral phase. A brief description of the plagioclase series is provided in Sect. 3.1, and the continuous solid solutions between the two end-members of the series, albite ($NaAlSi_3O_8$; Ab) and anorthite ($CaAl_2Si_2O_8$; An), are illustrated in Fig. 1.

The primary objective of this paper is to determine the extent to which the plagioclase Si–O–Si silicate network can be fully broken down by direct HNO_3 leaching. The secondary objective was to assess the degree of reactivity of Ca-bearing plagioclase (present as anorthite) with $(NH_4)_2SO_4$ during thermochemical processing, if any. For this purpose, a plagioclase concentrate was produced from a rock identified as coarsely grained pyroxenite, which was retrieved in situ from the southern sector of the eastern limb of the BIC, approximately 25 km south of the Two Rivers platinum mine from which tailings were used by Mohamed et al. [33–35].

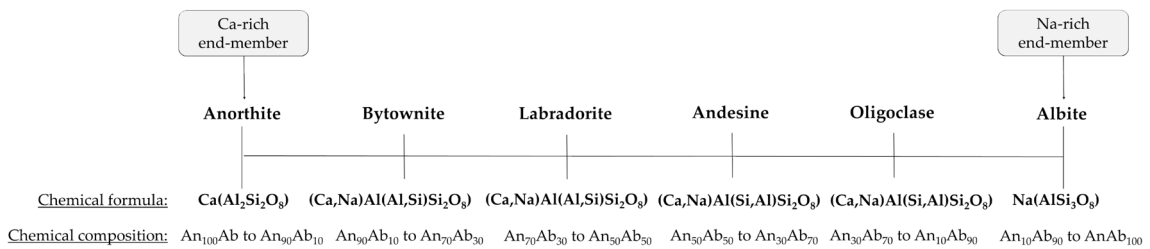

Fig. 1 Nomenclature and chemical formulae for the plagioclase feldspar series ranging between the Ca-rich end-member (anorthite) and the Na-rich end-member (albite)

2 Materials and methods

2.1 Preparation of the starting material

The preparation of the plagioclase concentrate was reported elsewhere [38]. In brief, the plagioclase concentrate was prepared from a single rock sample (Fig. S1) donated by the Booysendal North Mine, a platinum mining operation managed by Northam Platinum Ltd. The mine is situated in the southern sector of the eastern limb of the Bushveld Igneous Complex (BIC) in South Africa, 35 km from the town of Mashishing (previously known as Lydenburg) and 25 km south of the Two Rivers Platinum Mine, whose tailings were used in previous work [33–35]. The rock was retrieved in situ and identified as coarsely grained pyroxenite. Its bulk mineralogy consisted of enstatite (66 wt%), augite (7 wt%), plagioclase (12 wt%), hornblende (3 wt%), biotite (5 wt%), quartz (3 wt%), and talc (4 wt%) [38].

The rock could not be processed by hand due to the small size of the pyroxene crystals present in the sample. The whole rock was first processed using a jaw crusher to reduce its size from cobble-sized chunks to ca. 5 cm fragments (Supplementary Figure S1A). The fragments were further crushed to sizes <1 mm using a roll crusher. The cumulus plagioclase component was estimated to have a density of ca. 2.7 g cm^{-3} [23] and was subsequently separated from denser pyroxene grains (estimated density: 3.4 g cm^{-3} [23]), by density separation using bromoform (density of 2.9 g cm^{-3}) at ambient temperature (Supplementary Figure S1B). After separation, the two fractions (Supplementary Figure S1C) were thoroughly washed with acetone. This study reports only on the plagioclase-rich fraction, hereafter called 'plagioclase concentrate', which is denoted as *Plg-c*. All experiments were performed on a single batch of *Plg-c*. Representative homogeneous subsamples of *Plg-c* were obtained using a splitter. *Plg-c* was stable and did not require storage under controlled atmospheric conditions. Because of the small sample mass, all experiments were conducted in duplicate using a limited number of established experimental variables to evaluate the reactivity of the plagioclase concentrate during direct acidic leaching and during thermochemical treatment with $(NH_4)_2SO_4$ followed by leaching.

2.2 Methods

2.2.1 Thermochemical treatment

The plagioclase concentrate *Plg-c* was mixed thoroughly with $(NH_4)_2SO_4$ (reagent grade, ≥99%, Merck, South Africa) at a constant solid—solid mass ratio of 1:3 (m/m) using an established thermochemical treatment preparation method [33, 35]. The resulting mixtures were placed in fused quartz crucibles and subsequently heat-treated in a muffle furnace set at 550 °C for 45 min. The reaction products (hereafter denoted *Plg-*c_{tct1}) were allowed to cool to ambient temperature and ground using a mortar and pestle before characterization and subsequent leaching in water (uncontrolled pH) or acid (controlled pH). An outline of the thermochemical treatment process is provided in Fig. 2.

2.2.2 Cyclical thermochemical treatment

Cyclical thermochemical treatment experiments were completed on *Plg-c* to ascertain whether $(NH_4)_2SO_4$ could be a limiting factor during the thermochemical step and whether an excess of $(NH_4)_2SO_4$ can yield improved extraction efficiencies. For this purpose, *Plg-c* was mixed with $(NH_4)_2SO_4$ at a 1:3 (m/m) ratio and subsequently heat-treated in a muffle furnace at 550 °C for 45 min. The reaction product (*Plg-*c_{tct1}) resulting from this first cycle was weighed and then mixed with additional $(NH_4)_2SO_4$ in a 1:3 (m/m) ratio before being subjected to the same thermal treatment (i.e., 550 °C, 45 min), which yielded *Plg-*c_{tct2}. This cycle was repeated five times. The final reaction product (hereafter denoted *Plg-*c_{tct5}) was allowed to cool to ambient temperature. All samples were ground using a mortar and pestle and stored in a dessicator before characterization and subsequent leaching in water or acid. An outline of the different thermochemical treatment cycles is provided in Fig. 2.

2.2.3 Leaching procedure

Leaching of *Plg-c* (i.e., direct acid leaching) and *Plg-*c_{tct} (i.e., leaching after the thermochemical step) was performed using established leaching procedures [35]. Briefly, the procedure consisted of suspending *Plg-c* or *Plg-*c_{tct} in 500 mL of either distilled water (electrical conductivity: 19 ± 2 µS cm^{-1}) or 0.63 M HNO_3 solution at 95 °C under continuous stirring at a

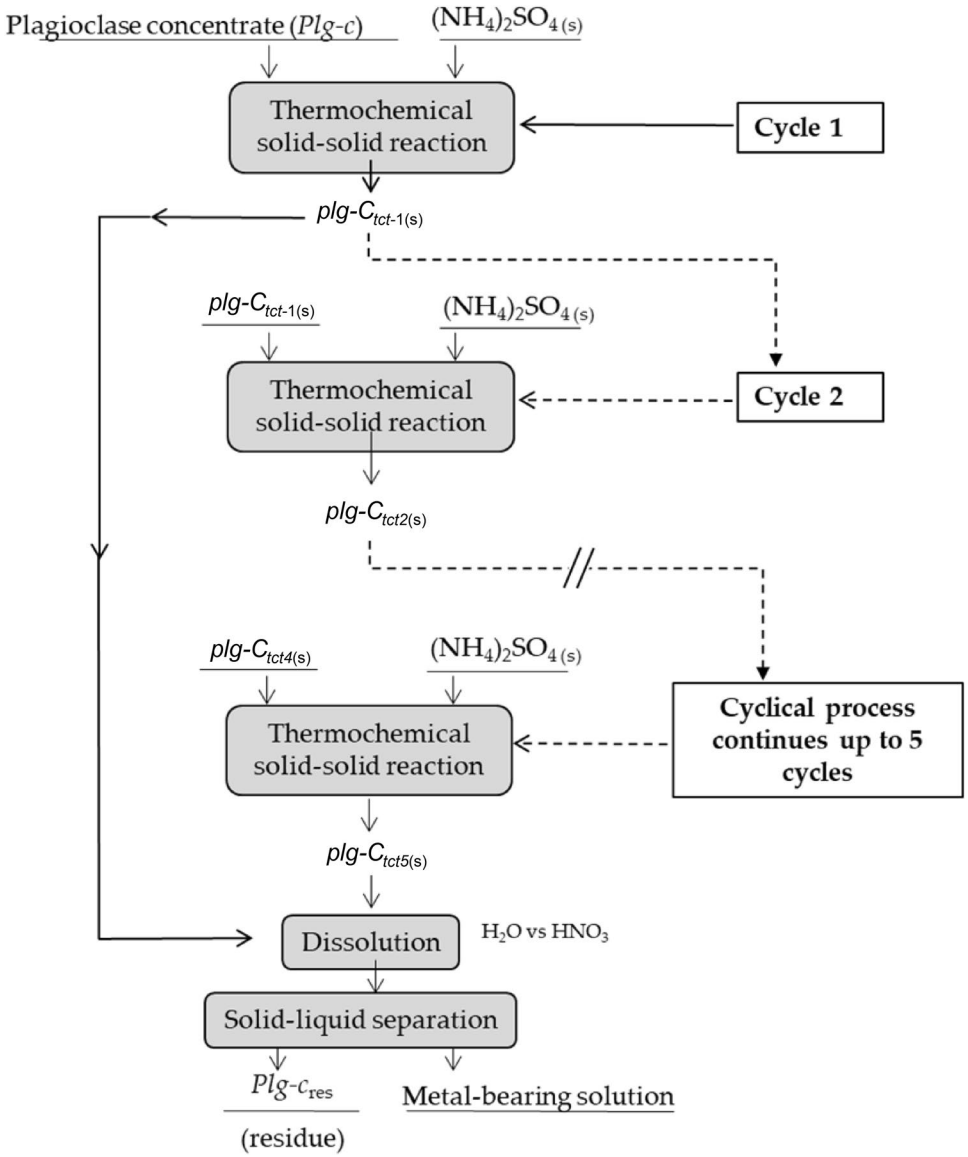

Fig. 2 Flow diagram for the multistage extraction process for the plagioclase concentrate using different thermochemical treatment cycles. The solid line indicates a single-cycle thermochemical treatment process. The dashed line indicates the 5-cycle thermochemical treatment process

constant speed of 850 rpm using a mechanical overhead stirrer (WiseStir HS30D, Wisd Lab Instruments) fitted with a 50 mm^3 bladed propeller-type impeller to maintain the particles in suspension for 6 h. The duration of direct acid leaching of *Plg-c* was also extended to 24 h to collect additional data on the dissolution of the plagioclase silicate network in acidic media. At the end of the leaching period, the solution pH and electrical conductivity (EC) of the leachates in distilled water were measured using a Hanna HI 2829 multiparameter logger. The solution pH and EC could not be measured for the leaching experiments conducted in HNO_3 because of the presence of HNO_3, which caused the solution conductivity to be greater than the maximum permissible measuring range of the logger (i.e., >200 mS cm^{-1}). An HNO_3 concentration of 0.63 M was selected because it was previously shown to prevent the formation of secondary iron precipitates during leaching [35]. The leachates were then filtered using Sartorius polycarbonate track-etch membranes (pore diameter of 0.4 µm) under reduced pressure and subsequently analyzed for their major element contents (Al, Ca, Na, Si, Fe, and Mg) by inductively coupled plasma—optical emission spectrometry (ICP-OES) at an accredited laboratory (Waterlab Pty Ltd, Pretoria, South Africa).

The results from the ICP analyses were used to calculate the elemental extraction efficiencies for the different treatment procedures. A subsample of the distilled water was submitted as a blank and analyzed by ICP for its metal content. The elemental concentrations were <1 mg/L for all the elements except for K and Na, which were ca. 7 and 10 mg/L, respectively. The presence of these elements accounted for the alkalinity of the water, which had a pH of ca. 8. The

elemental extraction efficiencies were calculated after subtracting the values obtained from the blank sample from the experimental values obtained for each element.

2.2.4 Characterization of solid materials

The elemental compositions of the solid materials were obtained using X-ray fluorescence (XRF) fused bead analysis (PANanalytical Axios X-ray fluorescence spectrometer equipped with a 4 kW Rh tube). Elemental analysis to determine the sulfur content of solids was conducted using a ThermoScientific Flash 2000 elemental analyzer.

The mineralogical compositions were determined using XRD (PANalytical X'Pert Pro powder diffractometer in the θ–θ configuration with an X'Celerator detector and variable divergence and fixed receiving slits with Fe-filtered Co-Kα radiation ($\lambda = 1.789$ Å)). For XRD analysis, the samples were prepared according to the standardized PA nanofibrous backloading system, which provides a nearly random distribution of the particles. The mineralogy was determined by selecting the best–fitting pattern from the ICSD database to the measured diffraction pattern. The relative phase concentrations were estimated using the Rietveld method with X'Pert Highscore Plus software.

Field-emission scanning electron micrographs (FE-SEM) were collected using a Zeiss Gemini Ultra Plus FEG SEM with an EDS detector operating under high-vacuum conditions with an accelerating voltage of 1.0 kV to obtain information on the morphologies of all the solid materials. The samples were mounted on a metal substrate using double-sided carbon tape and subsequently sputter-coated with a thin, conductive layer of carbon using an Emitech K550X coater (Ashford, England).

Thermogravimetry/differential thermal analysis (TG and DTA) analyses were performed on a TA Instruments SDT Q600 instrument in duplicate to confirm the observed effects. Approximately 20 mg of sample was heated from 25 to 1400 °C at a heating rate of 10 °C per min in alumina pans under a dynamic air atmosphere controlled at a flow rate of 100 ml per min.

3 Results and discussion

3.1 Characterization of the starting material

Feldspars are the most abundant mineral group in igneous and metamorphic rocks [18]. They are a series of silicate minerals divided into two main subgroups: (1) K-feldspar or alkali feldspars and (2) plagioclase feldspars. Alkali feldspars range in composition between the K end-member, orthoclase ($KAlSi_3O_8$), and the Na end-member, albite ($NaAlSi_3O_8$; Ab). The plagioclase series comprises a continuous solid solution (Fig. 1) between the two end-members, albite ($NaAlSi_3O_8$; Ab) and anorthite ($CaAl_2Si_2O_8$; An). The plagioclase series is subdivided into six intermediate compositional varieties, given specific nomenclature depending on the mole percentage of Na and Ca. The Na-rich end-member, albite (Ab), may contain up to 10 mol percent of the anorthite (An_{10}) component; and the Ca-rich end-member, anorthite (An), may range between Ab_{10} and Ab_0. Intermediate species include oligoclase (Ab_{90}–Ab_{70}), andesine (Ab_{70}–Ab_{50}), labradorite (Ab_{50}–Ab_{30}) and bytownite (Ab_{30}–Ab_{10}) [6, 23].

In general, plagioclase feldspars belong to the subclass "tectosilicates" and conform to a triclinic crystal structure. Tectosilicates are framework silicates comprising a three-dimensional (3D) SiO_4 and AlO_4 tetrahedral framework. Each tetrahedron consists of a Si or Al atom bonded to four O atoms and positively charged cations, occupying the framework's larger interstices [9]. The degree of ordering of the cations primarily depends on the conditions during formation, i.e., the crystallization temperature and thermal history of the feldspar. The substitution of Al^{3+} for Si^{4+} requires a charge balance to be maintained and is attained by incorporating monovalent and divalent cations such as K^+, Na^+ and/or Ca^{2+}. The substitution of one Al^{3+} for Si^{4+} allows the incorporation of one Na^+ or K^+ cation into the lattice structure, whereas substituting two Al^{3+} cations for Si^{4+} allows one Ca^{2+} cation to be incorporated into the lattice structure [23]. Elements such as Ti, Fe, Mn, Mg, Ba and Sr may also be present in limited amounts, either as impurities or as a replacement for Ca in plagioclase [21].

Plg-c was predominantly composed of SiO_2 (55.0 wt%), Al_2O_3 (22.2 wt%), CaO (10.5 wt%), Na_2O (3.2 wt%), MgO (3.5 wt%) and Fe_2O_3 (2.7 wt%) (Table 1). The sample exhibited a negative loss on ignition (LOI = −1.1), which is typically due to the oxidation of Fe^{2+} to Fe^{3+} (FeO to Fe_2O_3) during analysis. Similar observations were previously made for Fe-rich mine tailings obtained from the BIC [35] and for coal fly ash [47]. The low Na_2O content of the samples suggested that the plagioclase mineral phase may have been predominantly present as a Ca-rich end-member (Fig. 1).

Table 1 Chemical composition of *Plg-c* (XRF, oxide wt%)

SiO_2	Al_2O_3	CaO	MgO	Na_2O	Fe_2O_3 (total)	K_2O	Other elements	LOI[a]
55.6	22.4	10.6	3.6	3.2	2.7	0.7	1.2	−1.1

[a]LOI: loss on ignition

Table 2 Mineralogical composition of the plagioclase concentrate (*Plg-c*)

Mineral group (mineral)	Ideal chemical composition	Abundance (wt%)
Plagioclase	$(Na, Ca)Al_{1-2}Si_{3-2}O_8$[a]	78
Orthopyroxene	$(Mg, Fe)_2Si_2O_6$[b]	9
Quartz	SiO_2	13

[a]Elements such as Ti, $Fe^{2+/3+}$, Mn, Mg, Ba and Sr may also substitute for Ca in the plagioclase feldspar series [21]

[b]Minerals of the orthopyroxene group range from pure Mg end-member, enstatite ($Mg_2Si_2O_6$) to the Fe end-member, ferrosilite ($Fe^{2+}{}_2Si_2O_6$). Orthopyroxenes may be represented by the generic formula $XYSi_2O_6$, where X and Y may be occupied by Mg, Fe^{2+}/Fe^{3+}, Ca, Al, Cr, Ti, Mn and Na [12]

The mineralogy of *Plg-c* consisted of three crystalline phases: plagioclase (78 wt%), orthopyroxene (in the form of enstatite; 9 wt%) and quartz (13 wt%) (Table 2). These results confirmed the effectiveness of the separation procedure, which produced a sample fraction with a high proportion of plagioclase (78 wt%) in comparison to the parent bulk rock (11 wt%) from which it was derived.

The thermogram of untreated *Plg-c* (Fig. 3) was mainly constant, indicating that the mineral phases present in *Plg-c* are thermally stable up to 1000 °C. The slight mass gain (ca. 1%) observed at ~ 1 250 °C was correlated with the negative LOI value and indicated the oxidation of Fe.

3.2 Characterization of thermochemically treated *Plg-c*

TGA was used to determine the thermal stability and phase transformations of *Plg-*c_{tct1} and *Plg-*c_{tct5}. Based on previous studies [8, 33, 35, 37], reactions between some silicate minerals (e.g., lizardite, kaolinite, serpentinite) and $(NH_4)_2SO_4$ during thermochemical treatment can lead to the formation of soluble metal sulfate species, whereas mineral phases such as talc have been shown to be nonreactive [8].

In contrast to the mostly horizontal thermograms observed for *Plg-c*, those of *Plg-*c_{tct1} and *Plg-*c_{tct5} displayed several mass loss steps that followed a similar trend for the two samples (Fig. 3A, B). The mass loss up to 200 °C corresponded to the liberation of water due to dehydration of hygroscopic metal sulfate hydrate species [35]. The mass loss transitions observed between 400 and 800 °C were attributed to the decomposition of Fe and Al-sulfate species, for which the onset of decomposition typically occurs between 500 and 600 °C [2, 44]. Additional mass loss events were observed between 800 and 1200 °C, which corresponded to the decomposition of magnesium sulfate and calcium sulfate, which are known to have onset temperatures of ca. 850 °C [44] and 1000 °C [13], respectively. The nearly identical mass loss curves observed for *Plg-*c_{tct1} and *Plg-*c_{tct5} above 200 °C indicated that increasing the number of cycles during the thermochemical treatment did not improve the conversion of the metals contained in *Plg-c* into metal sulfate species and suggested that the products enclosed a similar amount of sulfate-containing phases. This result was confirmed with sulphur analyses, which indicated that the sulphur contents of *Plg-*c_{tct1} and *Plg-*c_{tct5} were 5 ± 1% and 4 ± 1%, respectively.

XRD of *Plg-*c_{tct} was performed to assess the presence of unreacted reactants and confirm the formation of new mineral phases following one or five cycles of thermochemical treatment (Table 3; Fig. 4), as suggested by TGA. XRD identified aluminum sulfate (millosevichite; $(Al,Fe)_2(SO_4)_3$) and calcium sulfate (anhydrite; $CaSO_4$) as newly formed mineral phases. Millosevichite was observed in both *Plg-*c_{tct1} and *Plg-*c_{tct5}, but its content in relation to the total crystalline phases increased from 4 to 10% with an increase in the number of cycles. The proportion of anhydrite, however, remained the same regardless of the number of cycles. The TGA results suggested the presence of magnesium sulfate, although such phases could not be identified by XRD. The relative phase proportion of plagioclase remained high in both *Plg-*c_{tct1} and *Plg-*c_{tct5}, which indicated a limited reaction between plagioclase and $(NH_4)_2SO_4$ during thermochemical treatment. This result suggested that a reaction between plagioclase and $(NH_4)_2SO_4$ may have

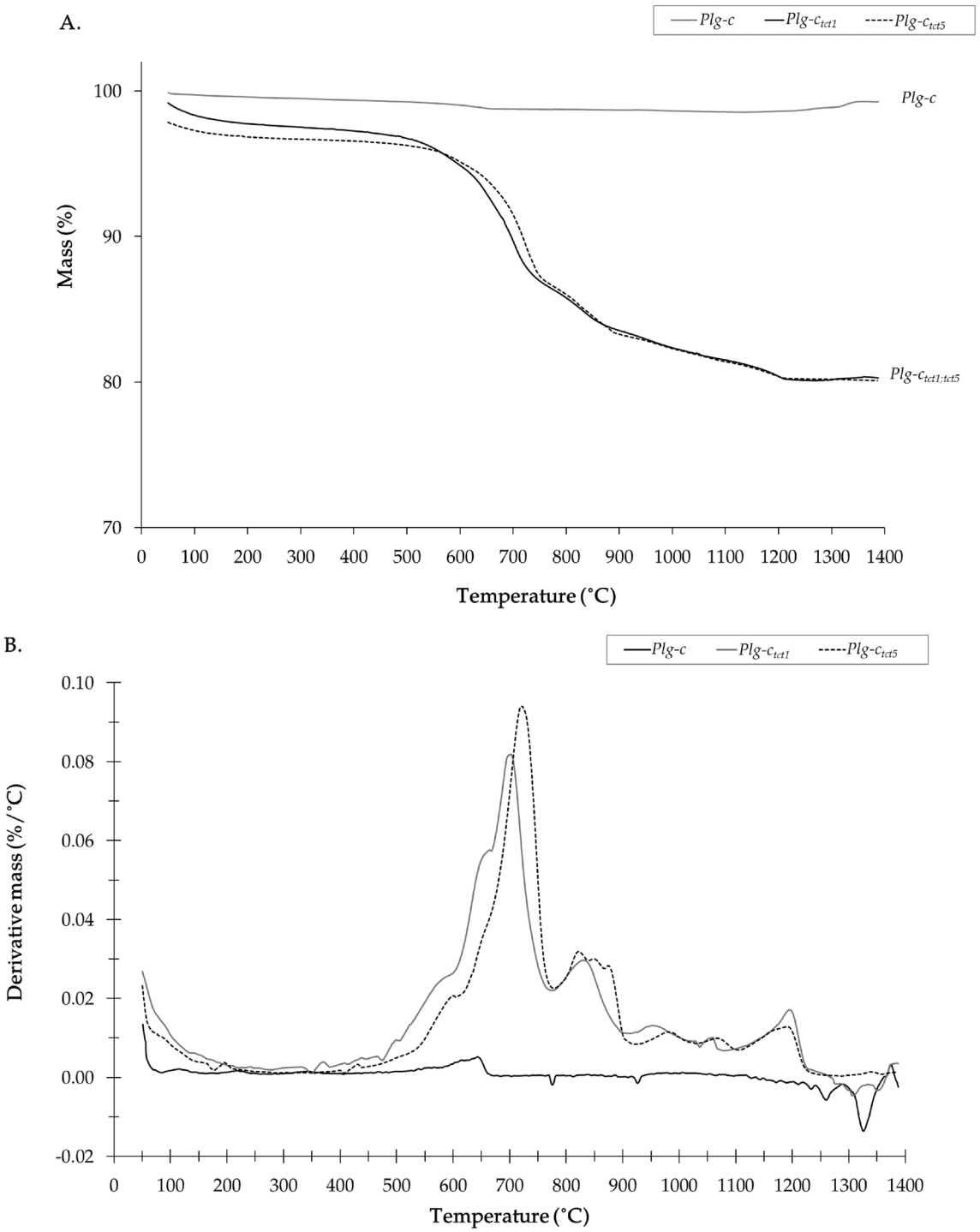

Fig. 3 TGA (**A**) and DTG (**B**) curves of untreated *Plg-c* and *Plg-*c_{tct} generated via the thermochemical treatment of *Plg-c* with $(NH_4)_2SO_4$ at 550 °C for one cycle (*Plg-*c_{tct1}) and five cycles (*Plg-*c_{tct5})

been thermochemically favorable, albeit with slow kinetics. It is conceivable that the plagioclase phase could react with AS further if a very high number of cycles is applied and if the treatment temperature is decreased from 500 to 400–450 °C to maximize the contact time between the sample and AS, but the energy penalty would be extensive.

Although no new Fe- or Mg-bearing sulfate phases could be identified by XRD, elemental substitution or solid solutions in the newly formed phases and the presence of isostructural mineral phases were most likely. For instance, millosevichite is known to be an Al analog of the mineral mikasaite $Fe_2(SO_4)_3$, in which Al and Fe can substitute for

Table 3 Mineralogical composition of *Plg-c*, *Plg-c*$_{tct1}$ and *Plg-c*$_{tct5}$

Mineral group (mineral)	Ideal chemical composition	Abundance (wt%)		
		Plg-c	*Plg* − c_{tct1}	*Plg* − c_{tct5}
Plagioclase (anorthite)	$(Na, Ca)Al_{1-2}Si_{3-2}O_8$	78	71	68
Orthopyroxene (enstatite)	$(Mg, Fe)Si_2O_6$	9	7	6
Quartz	SiO_2	13	15	12
Anhydrite	$CaSO_4$	–	4	4
Millosevichite (Al and/or Fe sulphate)	$(Al, Fe)_2(SO_4)_3$	–	4	10

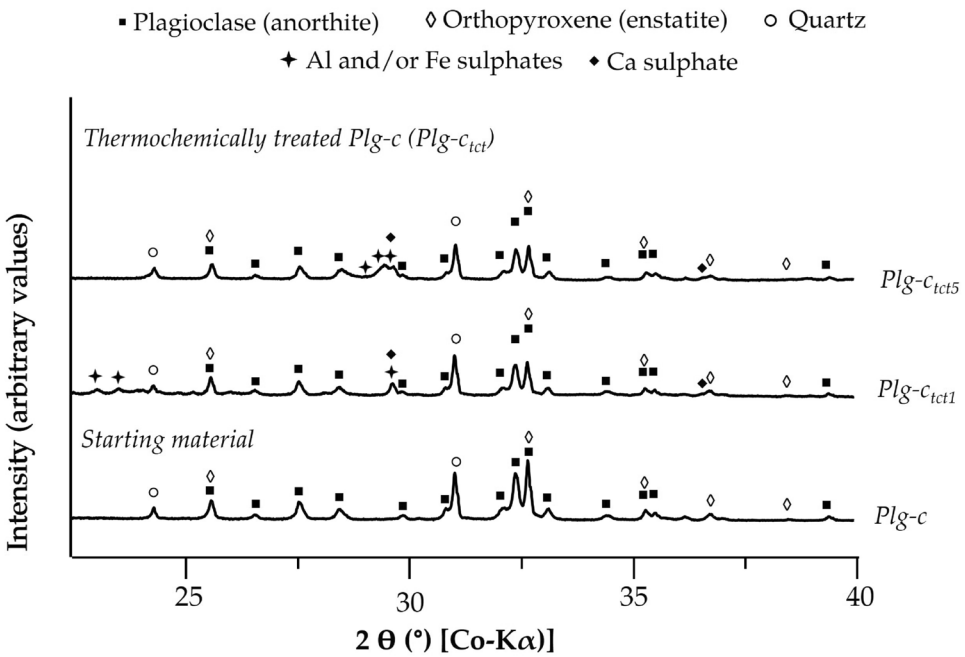

Fig. 4 Mineralogical composition of *Plg-c*, *Plg-c*$_{tct1}$ and *Plg-c*$_{tct5}$

each other in two mineral structures [29, 30, 41]. These two mineral phases have been reported to have hygroscopic properties due to their strong deliquescence [24, 30], which was observed in the TGA curves (Fig. 3) for both *Plg-c*$_{tct1}$ and *Plg-c*$_{tct5}$.

The presence of newly formed sulfate species in *Plg-c*$_{tct}$ was further confirmed using FE-SEM (Fig. 5). Untreated *Plg-c* was made up of irregularly shaped particles of varying sizes in the submicron and micron ranges (Fig. 5A). *Plg-c*$_{tct}$ contained unreacted, irregularly shaped particles surrounded by numerous newly formed and near-cubical hexagonal structures. The hexagonal structures were interlocked plate-like particles that formed clusters of varying sizes (Fig. 5B, C). The thickness of these hexagonal structures was less than 10 µm. Submicron cubic-like structures were also present at the surface of these hexagons (Fig. 5E, F), although it was not possible to ascertain whether they were precursors to the hexagonal structures or were the anhydrite phase identified by XRD. Anhydrite is an orthorhombic-cubic crystal system and is usually characterized by thick tabular shapes [21]. Similar mineral phases and morphologies were also observed in coal fly ash that had been thermochemically treated with $(NH_4)_2SO_4$ at similar temperatures [11]. The formation of hexagonal particles during the thermochemical treatment of PGE tailings and coal fly ash with $(NH_4)_2SO_4$ was previously attributed to metal (Fe, Al, Cr, and/or Mg) sulfates, which generally display hexagonal habits [11, 33, 35]. These results confirmed that the plagioclase and/or enstatite present in *Plg-c* reacted with $(NH_4)_2SO_4$ during the thermochemical treatment.

3.3 Elemental extraction

Elemental extraction efficiencies were assessed using a previously established method [33, 35], which consists of leaching the samples under continuous mixing conditions at 95 °C for 6 h to dissolve metal sulfates and prevent secondary mineral precipitation. The elemental extraction efficiencies of *Plg-c*, *Plg-c*$_{tct1}$ and *Plg-c*$_{tct5}$ were evaluated in two different leaching media: (1) distilled H_2O and (2) 0.63 M HNO_3.

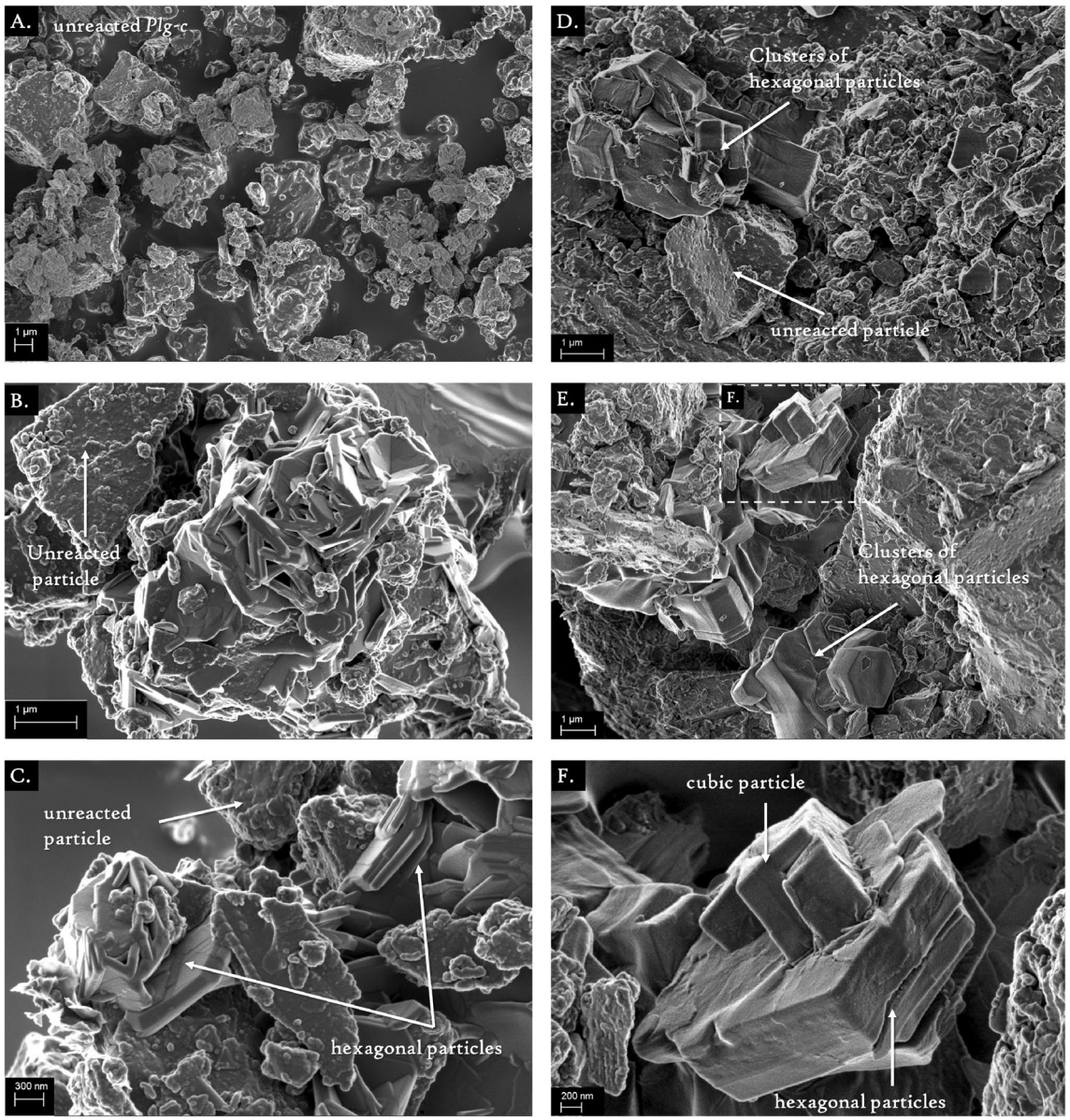

Fig. 5 FE-SEM images of untreated (**A**) and thermochemically treated *Plg-c* (**B**–**F**) using $(NH_4)_2SO_4$ at 550 °C. The predominant features of the samples are indicated with labeled arrows

3.3.1 Leaching in H_2O

Baseline leaching experiments were initially conducted in H_2O to assess and compare the leaching behavior of untreated *Plg-c* and treated *Plg-*c_{tct1} and *Plg-*c_{tct5}.

Plg-c: Leaching of *Plg-c* in H_2O was minimal. This was indicated by the near-neutral pH of the filtrate (7.8), the low EC (72 ± 4 µS cm^{-1}; Table 4) and the low elemental extraction efficiencies (<8%) obtained for all the elements, except for Na (18%) (Fig. 6A). The latter explained the slight increase in EC from ca. 19 µS cm^{-1} for H_2O to ca. 72 µS cm^{-1} for the filtrate.

Plg-c_{tct1} *and Plg-*c_{tct5}: The filtrates obtained from *Plg-*c_{tct1} and *Plg-*c_{tct5} were characterized by an acidic pH of 3.3–3.5 and higher EC values (285–359 µS cm^{-1}; Table 4), which provided the first indication of higher elemental extraction from *Plg-*c_{tct} than from *Plg-c*. This was supported by ICP, which confirmed higher elemental extraction of Fe (2–4%), Al (7–8%), Ca (13–17%), and Mg (33–41%); in contrast, very little extraction of Si was observed (<1%, Fig. 6A). These higher extraction efficiencies were attributed to the dissolution, either in full or in part, of sulfate species such as $CaSO_4$ and $(Al, Fe)_2(SO_4)_3$, which had formed during thermochemical treatment (Table 3). No difference was observed in the extraction efficiencies

Table 4 Solution pH and electrical conductivity (EC) after leaching of untreated *Plg-c* vs. thermochemically treated *Plg-*c_{tct1} and *Plg-*c_{tct5} in distilled water (1 g/500 ml, 95 °C, 850 rpm, 6 h; $n = 2$)

	pH	EC (µS cm^{-1})
Distilled water	8.0 ± 0	19 ± 2
Plg-c	7.8 ± 0.3	72 ± 4
Plg-c_{tct1}	3.5 ± 0.1	285 ± 40
Plg-c_{tct5}	3.3 ± 0	359 ± 35

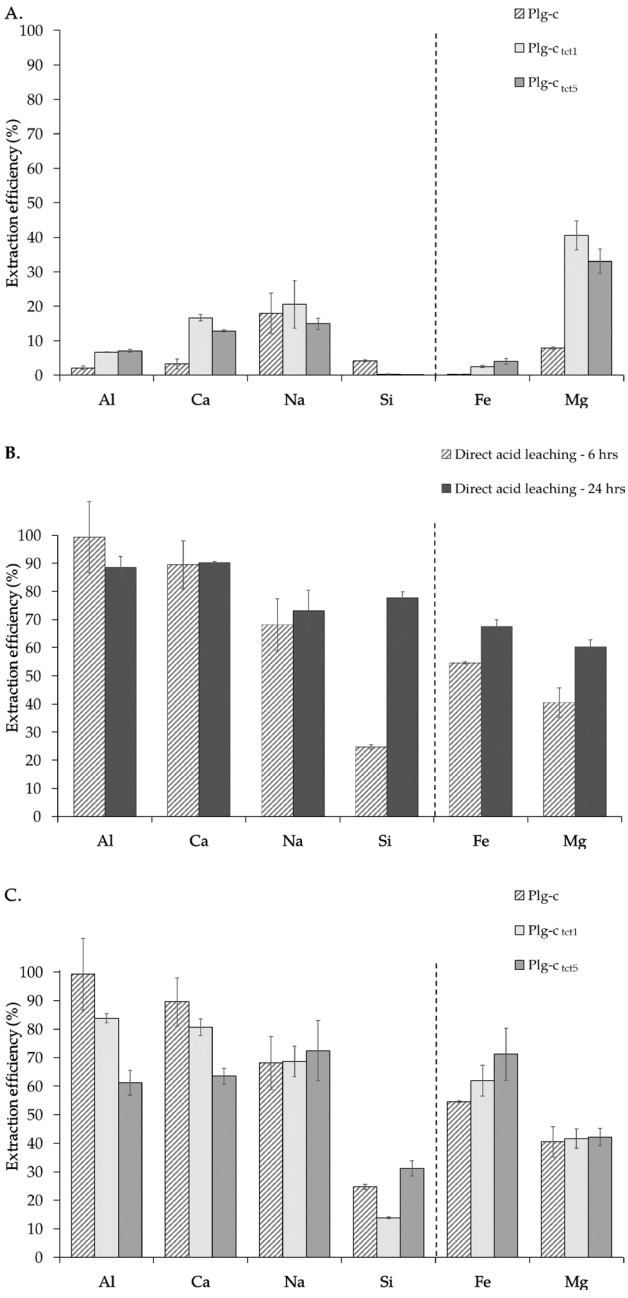

Fig. 6 Elemental extraction efficiencies following leaching of *Plg-c* and *Plg-*c_{tct} in (**A**) distilled water, (**B**) direct acid leaching of untreated *Plg-c* in 0.63 M HNO_3 (1 g/500 mL, 95 °C, 850 rpm, 6 h and 24 h; $n = 2$) and leaching of *Plg-c* and *Plg-*c_{tct} in **C** 0.63 M HNO_3 (1 g/500 mL, 95 °C, 850 rpm, 6 h; $n = 2$)

of Na when leached in H_2O or for the different cycles of thermochemical treatment. The elemental extraction efficiencies for Al, Na, Si and Fe from *Plg-*c_{tct5} remained similar to those from *Plg-*c_{tct1}, whereas those of Ca and Mg decreased from 17 to 13% and 41 to 33%, respectively. The increase in elemental extraction efficiencies following thermochemical treatment, particularly for Ca, Fe, and Mg, suggested some degree of reactivity of the plagioclase and perhaps enstatite mineral phases during thermochemical treatment with $(NH_4)_2SO_4$, although the extent could not be confirmed. Further

investigation is also required to ascertain whether the decrease in the solution pH to 3.3–3.5 due to the dissolution of sulfate species had any effect on the extraction efficiencies of some of the elements.

3.3.2 Leaching in HNO_3

Plg-c: Direct acid leaching of *Plg-c* in HNO_3 was performed to assess the extent of breakdown of the silicate network of plagioclase that can be achieved via direct acid leaching. Compared with H_2O, direct acid leaching improved the extent of elemental extraction for all elements (Fig. 6B). The elements contained in *Plg-c* could be categorized into three groups based on their susceptibility to acid extraction following the 6 h direct leaching process. Group 1 included the highly reactive main elements of the plagioclase phase (Al, Ca and Na with extraction efficiencies of ca. 95%, 89% and 81%, respectively) but excluded Si, whose extraction efficiency was limited to ca. 25%. Group 2 included elements that were predominantly present in the enstatite minerals (Mg and Fe with extraction efficiencies of ca. 41% and 55%, respectively). Group 3 was composed of slowly extractable Si, which was contained in both the plagioclase phase and the enstatite phase, but the structural silicate network in plagioclase was likely more acid soluble than that in enstatite. These differences in solubility were expected owing to differences in their structural make-ups. The plagioclase mineral structure consists of a 3-D framework of AlO_4 and SiO_2 tetrahedra, which are linked via Al–O–Si and Si–O–Si bonds [51]. The rate and mechanism of plagioclase dissolution are dependent on the composition and pH. In particular, the rate of dissolution increases with increasing anorthite content under acidic conditions [3, 7, 17, 19, 39, 51]. The dissolution of plagioclase proceeds with the initial removal of Na, Ca and Al atoms and the occurrence of a thin altered hydrous silicon dioxide surface layer [42], followed by the release of the surrounding isolated Si atoms. Less energy is required to break the Al–O–Si bonds relative to the Si–O–Si bonds [51]. In comparison, enstatite belongs to the inosilicate mineral class and comprises a single tetrahedral chain structure held together by magnesium octahedra. Oelkers and Schott [40] reported that the dissolution of enstatite occurs in two stages: (1) the breaking of Mg-O bonds and (2) the detachment of silica from tetrahedral chains. The breaking of the Mg-O bonds occurs rapidly and does not destroy the mineral structure,however, it allows for the release of the silica tetrahedral chains. This accounts for the preferential and faster release of Mg over Si from the enstatite mineral phase [27].

The duration of direct acid leaching of untreated *Plg-c* in HNO_3 increased from 6 to 24 h in an effort to improve the elemental extraction efficiency, particularly to specifically assess the susceptibility of the silicate networks formed by plagioclase and enstatite to extended acid extraction (Fig. 6B). The elemental (metallurgical) balance for the best *Plg-c* leaching in HNO_3 (i.e., 24 h) with 100 g of plagioclase concentrate is shown in Table 5. Increasing the duration of direct acid leaching from 6 to 24 h had no effect on the extraction of the group 1 elements (i.e., Al, Ca, and Na), whereas the extraction of Mg and Fe (Group 2) increased from ca. 41 to 60% and 55 to 68%, respectively. The extraction efficiency of Si (Group 3) tripled from ca. 25% to ca. 77%, which provided direct evidence of the progressive breakdown of one of the silicate networks contained in *Plg-c* when increasing the duration of direct acid leaching in HNO_3 from 6 to 24 h.

Plg-c_{tct1} and Plg-c_{tct5}: The dissolution of *Plg-*c_{tct1} in acid achieved greater elemental extraction for all the tested elements than did the leaching of *Plg-*c_{tct1} in H_2O (Fig. 6A vs. Figure 6C). The elemental extraction efficiencies increased between 14 and 77%, except for that of Mg, for which no significant differences were found when leached in either H_2O or acid. These results indicated that the Mg sulfate species readily dissolved in both H_2O and acid, whereas other metal sulfate species were more soluble in acid than in H_2O. The addition of a single-cycle thermochemical treatment step using $(NH_4)_2SO_4$ achieved lower extraction efficiencies for Al (84%), Ca (81%), and Si (14%) when leaching was performed in HNO_3 compared to direct acid leaching (Fig. 6C). The extraction efficiencies of Al, Ca, and Na (Group 1) showed a minor decrease between 9 and 6% compared to those of Si (Group 3), which decreased by 11%. The extraction efficiencies for Group 2 elements, Fe and Mg, increased slightly between 1 and

Table 5 Metallurgical balance based on the leaching of 100 g of untreated *Plg-c* in 0.63 M HNO_3 (1 g/500 mL, 95 °C, 850 rpm, 24 h; $n = 2$)

	Elemental composition (g/100 g plagioclase concentrate)					
	Si	Al	Ca	Na	Mg	Fe
Elemental composition of plagioclase concentrate (feed)	25.7	11.7	7.5	2.4	2.1	1.9
Elemental composition of leachate	20.0	10.4	6.8	1.7	1.3	1.3
Elemental composition of residue (calculated)	5.7	1.4	0.7	0.6	0.8	0.6
Recovery (%)	**77.7**	**88.4**	**90.2**	**73.1**	**60.3**	**67.6**

5%, respectively. The five cycles of thermochemical treatment prior to acid leaching exhibited a similar trend and resulted in lower extraction efficiencies for Al (61%) and Ca (63%) but an increase in Si (31%) extraction efficiency. The extent of Fe extraction was the highest after five cycles of thermochemical treatment, while no significant differences in the extraction efficiencies for Na and Mg were found with respect to acid dissolution and different cycles of thermochemical treatment. Given that plagioclase is the predominant mineral phase in *Plg-c*, these results suggested that the dissolution of the plagioclase phase most likely contributed to Al, Ca, Na and Si coextraction into solution during acidic leaching.

The decrease in extraction efficiencies in HNO_3 following thermochemical treatment may be due to the lower solubility of metal sulfate species such as $CaSO_4$, which is known to be soluble in acids; however, it is only slightly soluble in water and decreases with increasing temperature [21]. Alternatively, the temperature applied during the five-cycle thermochemical treatment may have resulted in the formation of (intermediate) metal sulfate species, which are less soluble in acids [11, 45]. Studies have also shown that the presence of epitaxial crystal growth or the formation of a passivating layer on mineral surfaces due to the precipitation of secondary minerals may limit transport properties and affect the mineral dissolution rate [5, 20, 46]. This phenomenon may explain the decrease in extraction efficiency obtained after the various cycles of thermochemical treatment. However, this could not be ascertained.

3.4 Characterization of residues

XRD and sulfur content analyses of the *Plg-*c_{res} following the leaching of *Plg-c*, *Plg-*c_{tct1} and *Plg-*c_{tct5} in distilled H_2O and HNO_3 were conducted to assess whether mineralogical changes had occurred following leaching with and without thermochemical treatment. For clarity, the XRD data are presented in two separate ways to take into consideration mass losses following leaching when comparing datasets. Figure 7A displays the XRD diffractograms, whereas Fig. 7B shows the normalized phase proportions (expressed in wt%) obtained from XRD in relation to the solid masses of the starting material (*Plg-c*) and the residues (*Plg-*c_{res}, *Plg-*c_{1res} and *Plg-*c_{5res}). For instance, the broad bar with the white background reported for *Plg-c* has a height of 1.0 along the y-axis, which indicates a starting mass of 100%. In comparison, the bar reported for the residue *Plg-*c_{res} (6 h) has a height of approximately 0.6, which indicates a mass loss of 40% compared to the starting mass of *Plg-c*. The adoption of this approach to represent and interpret these datasets was important since it highlighted that the mineralogical composition of the starting material and the residue was similar, although the mass of material recovered after leaching was 40% lower.

These data, when combined with the extraction data, helped to better understand the reactivities of plagioclase and enstatite under the experimental conditions investigated.

3.4.1 Residues from H_2O leaching

The mineralogical compositions of the residues generated by H_2O leaching and the approximate proportions between crystalline phases were similar, if not identical, to those of untreated *Plg-c*, regardless of whether *Plg-c* underwent thermochemical treatment before H_2O leaching. Although XRD was able to confirm the dissolution of most, if not all, of the metal sulfate species formed during thermochemical treatment by H_2O leaching, the technique was unable to identify changes in the structural silicate networks of plagioclase and enstatite, even though ICP demonstrated some degree of metal extraction (e.g., 7–8% Al; 13–17% Ca; 33–41% Mg; Fig. 6A). The results highlighted the usefulness and limitations of XRD when investigating the early stages of elemental metal extraction from silicate networks.

Figure 7B shows mass losses ranging between ca. 38% and 46% when H_2O leaching was applied to the samples with and without thermochemical treatment. However, mass losses within this range are likely caused by experimental artifacts (i.e., unavoidable cumulative material loss throughout the experimental steps) due to the very small amount of starting material used in the experiments. Despite this possible limitation in the usefulness of mass measurements due to a lack of sensitivity, the test is simple and inexpensive and can generate useful data, such as those obtained in the case of acid leaching of *Plg-c* for 24 h, where a mass loss of 86% was consistently obtained (Fig. 7B).

3.4.2 Residues from direct acid leaching of *Plg-c*

Section 3.3.2. reported high (>81%) extraction of Group 1 elements (Al, Ca, and Na associated with the plagioclase phase) and intermediate (41–65%) extraction of Group 2 elements (Mg and Fe associated with the enstatite phase) following direct acid leaching for 6–24 h, which indicated that plagioclase was more reactive than enstatite when suspended in

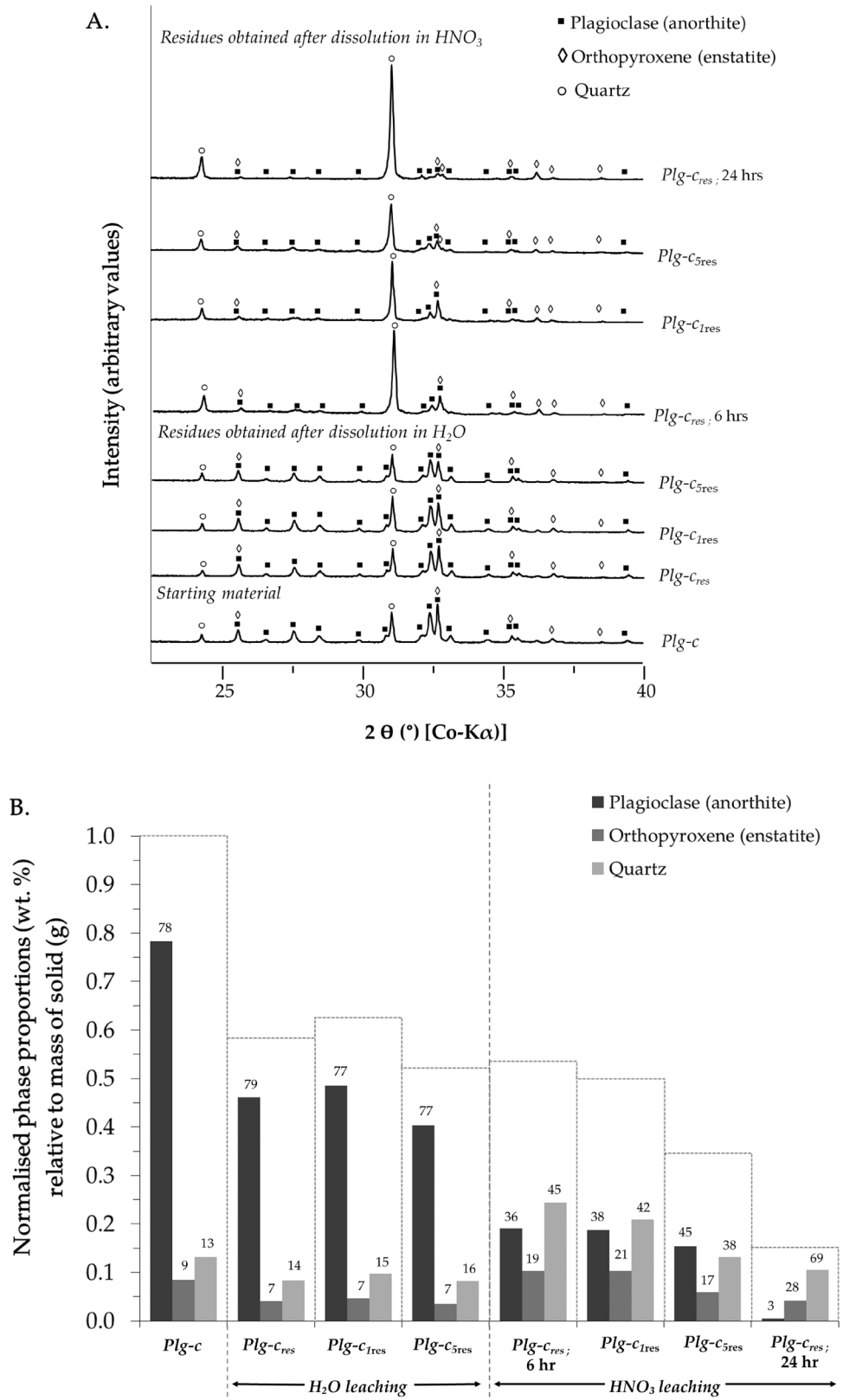

Fig. 7 **A** XRD diffractograms and **B** normalized phase proportions (wt%) obtained by XRD relative to the solid mass (g) before and after leaching of *Plg-c* and *Plg-c*$_{tct}$ in H_2O, 0.63 M HNO_3 (dotted lines in **B** indicate mass of residue)

acid. The extraction data also demonstrated a substantial increase in Si extraction from ca. 21 to ca. 80% when leaching had been extended from 6 to 24 h, which strongly suggested the destruction of one of the silicate networks contained in *Plg-c*. The latter was confirmed by XRD (Fig. 7), which revealed a considerable decrease in the plagioclase-to-quartz

ratio from 6.0 in untreated *Plg-c* to 0.8 and 0.04 in the residues after 6 h and 24 h of leaching, respectively. In contrast, the enstatite-to-quartz ratio was also reduced from 0.7 in untreated *Plg-c* to a constant value of ca. 0.4 in the residues after 6 h and 24 h of leaching, although to a much lesser extent than the plagioclase-to-quartz ratio. These results provided strong evidence that most of the Si extracted between 6 and 24 h originated from plagioclase rather than from enstatite. The dissolution of a large proportion of plagioclase, the main component of *Plg-c*, was further supported by the 86% mass loss recorded after 24 h of leaching.

3.4.3 Acid-leached residues of thermochemically treated *Plg-c*

XRD confirmed the dissolution of most, if not all, of the metal sulfate species formed during the thermochemical treatment by acid leaching (Fig. 7). This process did not improve the reactivity of plagioclase during the acid leaching step, as indicated by the similar plagioclase-to-quartz ratio of 0.8 for the residue after 6 h of direct acid leaching, compared to the ratio of 0.9–1.2 for *Plg-c*$_{1res}$ and *Plg-c*$_{5res}$ (Fig. 7). The enstatite-to-quartz ratio remained fairly constant at 0.4–0.5 for the residues after 6 h of direct acid leaching as well as for *Plg-c*$_{1res}$ and *Plg-c*$_{5res}$.

3.5 Quantification of plagioclase extraction

The theoretical chemical formula of plagioclase was calculated to quantify the contributions of Al, Ca, Na and Si from the plagioclase phase to the chemical composition of the filtrates. To complete the quantification, two assumptions were made: (1) all elemental Na and Ca measured in *Plg-c* by XRF are contained in the plagioclase phase, and (2) there is no elemental substitution for Ca and Na by impurities or other elements such as Ti, Fe, Mn, Mg, Ba and Sr. The theoretical chemical formula was calculated using the basic principles of mineral formula calculations based on Pauling's rules [23], ensuring charge balance and chemical variation in mineral compositions. Based on the ideal chemical formula for plagioclase ((Na, Ca)$Al_{1\text{-}2}Si_{3\text{-}2}O_8$), the theoretical formula of plagioclase in *Plg-c* was calculated to be $(Na_{0.35}Ca_{0.65})Al_{1.65}Si_{2.35}O_8$) or $An_{65}Ab_{35}$. Plagioclase in *Plg-c* is classified as labradorite based on the mole percentages of Na and Ca (Fig. 1). The molar mass of plagioclase was calculated based on the theoretical chemical formula of plagioclase present in *Plg-c* according to Eq. (1), where M_m refers to the molar mass and n refers to the number of moles:

$$M_m\text{of plagioclase} = \sum (M_m\text{of element} \times n\text{ of element in theoretical formula}) \tag{1}$$

The number of moles of plagioclase in solution was calculated according to Eq. (2):

$$n\text{ of plagioclase in solution} = \frac{\text{mass of starting material} \times \%\text{ plagioclase in starting material}}{M_m\text{of plagioclase}} \tag{2}$$

The theoretical elemental concentration leached into solution from the plagioclase phase in *Plg-c*, assuming 100% dissolution of the plagioclase phase, was calculated according to Eq. (3):

$$\text{elemental concentration(mol/L)} = n\text{ plagioclase in1 L solution} \times \frac{n\text{ of element}}{1\text{ mol plagioclase}} \tag{3}$$

The theoretical contributions of the elements dissolved in solution from the plagioclase phase present in *Plg-c* after 6 h and 24 h of direct acid leaching were compared to the values obtained experimentally (Fig. 8). These correlations suggested that these elements were progressively extracted from *Plg-c* after 6 h and 24 h of acid leaching. This trend follows the progressive depolymerization dissolution mechanism, favoring the preferential hydrolysis of Al–O–Si bonds over the Si-rich surface layer [3] and accounting for the rapid dissolution of interstitial cations, Ca and Na, from the surface of the mineral [51]. The deviation in Si extraction indicates nonstoichiometric dissolution, particularly after 6 h, which indicates slower dissolution kinetics of Si from the silicate network, whereas stoichiometric dissolution between Ca, Al and Si was reached after 24 h.

The preferential dissolution of Al, Ca, and Na over Si in the first 6 h of leaching resulted in a Si-rich structure whose Si–O-Si bonds broke down at a slower rate during the 24 h period [3, 5, 7]. This explains the high proportion of anorthite identified in *Plg-c*$_{res}$ after 6 h of leaching despite high elemental extraction efficiencies for Al, Ca, and Na compared to 24 h of leaching. The Si extraction efficiency after 24 h of leaching (400 mg/L; i.e., 14 mmol/L) deviated very slightly from the

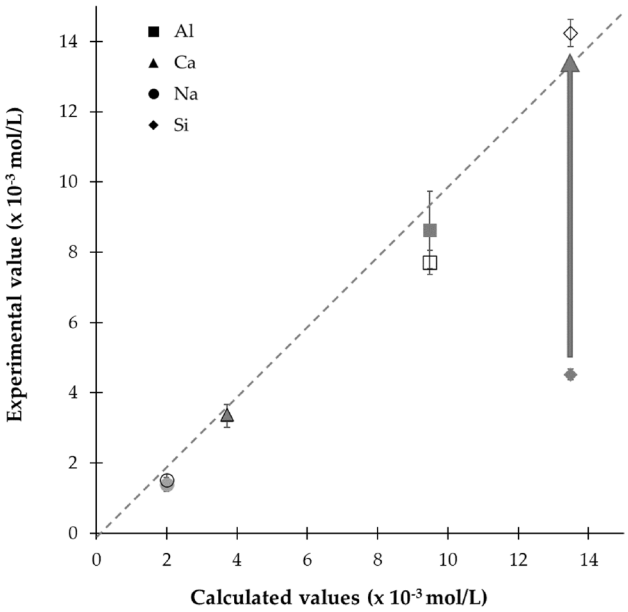

Fig. 8 Correlation between the theoretically calculated vs. experimentally obtained elemental contributions of Al, Ca, Na, and Si from the plagioclase mineral phase present in the *Plg-c* after acid leaching over 6 h (closed symbols) and 24 h (open symbols) ($n = 2$)

calculated value of 379 mg/L (i.e., 13 mmol/L) (Fig. 8), but this deviation was too low to suggest Si extraction from phases other than plagioclase. Furthermore, these experiments confirmed that 6 h is not sufficient to fully dissolve plagioclase under the tested temperature and acidic conditions.

The Ca:Al and Si:Al mole ratios of the leachates were compared to better understand the leaching behavior of the plagioclase phase. The Ca:Al mole ratio in solution deviated only slightly from the calculated theoretical value (Ca:Al = 0.4). This suggested that Al and Ca dissolved stoichiometrically over the 6 h (Ca:Al = 0.4) and 24 h (Ca:Al = 0.4) leaching durations. In comparison, the Si:Al mole ratios varied significantly according to the calculated theoretical formula (Si:Al = 1.4). The Si:Al mole ratio in solution after 6 h of dissolution (Si:Al = 0.5) compared to 24 h (Si:Al = 1.8) confirmed a slower dissolution rate for Si than for Al, which was slightly greater than the calculated stoichiometric mole ratio of 1.4. This confirmed the preferential leaching of Al, Ca and Na from the plagioclase structure and the lower Si extraction rate into solution.

Several cautions with respect to the interpretation of the above data were noted. This included (1) the assumptions used to calculate the theoretical formula of the plagioclase present in *Plg-c*; (2) the calculated values provided a qualitative view of the contribution of Al, Ca, Na, and Si dissolved in solution from the plagioclase phase present in *Plg-c*; (3) no direct information was obtained from the surface of the particles remaining in the residue; and (4) the limitations of the accuracy of the calculated values. The latter may include systematic errors arising from, e.g., instrumental errors or method errors proportional to the sample size [43].

3.6 Recommended selection criteria for industrial validation

Although it is premature to extrapolate the results of the direct acid leaching process developed on the plagioclase concentrate to plagioclase-bearing mine waste residues, a preliminary set of key performance indicators (KPIs) was suggested (Table 6) to help identify the critical metrics that would assist with evaluating the efficiency, effectiveness, and environmental impact of the leaching process for further development and validation. Specific targets on each KPI would have to be established via a techno-economic study performed on a case-by-case basis before upscaling.

4 Conclusions

This study investigated the reactivity of a plagioclase concentrate in acidic solution versus thermochemical processing with $(NH_4)_2SO_4$. Plagioclase was found to have limited reactivity with $(NH_4)_2SO_4$ when subjected to thermochemical treatment. Direct acid leaching allowed for the complete dissolution of plagioclase under the experimental conditions tested. However, longer durations are required to achieve stoichiometric dissolution of elements and to break the Si–O-Si

Table 6 Preliminary set of key performance indicators for the evaluation of the efficiency, effectiveness, and environmental impact of the leaching process for further development and validation

KPI category	KPI	Measurement unit	Data collection method
Leaching efficiency	Percentage of target substances leached (Ca, Al, Si)	% Ca, Al, Si	Laboratory analysis
Leaching efficiency	Process yield	% Ca, Al, Si	Mass balance calculations
Leaching efficiency	Leaching rate of Ca, Al and Si	mg element/L per hour	Continuous monitoring
Leaching efficiency	Mass of contaminants (e.g. Fe)	Total mg element/L	Laboratory analysis
Chemical consumption	Amount of leaching agent used	kg or L	Inventory tracking
Process optimization	Processing duration	Hours or days	Process logs
Process optimization	Energy consumption	kWh	Energy meter
Economic metrics	Cost per unit of leached Si	$/kg	Financial records
Economic metrics	Overall cost of the leaching process	$	Financial records
Environmental impact	Waste generation	L or kg of waste per kg of solid residue processed	Waste audits

covalent bonds to release Si into the solution. The direct acid extraction process offers the significant advantage of recovering major elements (Al, Ca, and Si) from the plagioclase component of tailings in a readily available soluble form using a single processing step. Such leachates may represent suitable precursors for the preparation of value-added products, such as silica nanoparticles via a sol–gel route and calcium aluminate nanoparticles via solution combustion. Silica nanoparticles find industrial applications in a wide variety of fields including biomedicine, agriculture, environmental remediation, water purification and fruit preservation [22], whereas calcium aluminate nanoparticles are used in a wide range of applications such as the construction industry, ceramics, binders in refractory castable for steel industry, detectors, biomaterials and optical devices [1].

Acknowledgements The project was financially supported by the Council for Geoscience (CGS), the University of Pretoria (UP), and the National Research Foundation of South Africa (NRF) [96849:2015; 138020:2022; DAAD-NRF: 88119:2014]. Any opinion, finding, conclusion or recommendation expressed in this material is that of the authors, and the NRF does not accept any liability in this regard. The authors thank the Laboratory for Microscopy and Microanalysis of UP for technical assistance on the SEM, H. van der Poll and E. van Vuuren from the Chemistry Department at UP for their assistance with the sulphur analysis, and the late Prof Dr Herbert Pöllmann of the Department of Mineralogy and Geochemistry, Martin-Luther-University, Halle-Wittenberg, Germany for hosting ZHN and assisting with mineral separation. The authors thank the CGS and FJD for providing supervisory assistance, insight and expertise.

Author contributions S.M.: Conceptualization, Investigation, Methodology, Data curation, Formal analysis, Writing—original draft. E.M.vd.M: Supervision, Conceptualization, Funding acquisition, Validation, Resources, Writing—review & editing. Z.H.N.: Sampling, mineral separation, writing—reviewing and editing. W.A.: Funding acquisition, Sampling, Writing—editing. W.G.: Formal analysis—mineralogical composition analysis and interpretation. FJ.D: Supervision, Conceptualization, Funding acquisition, Validation, Resources, Writing—reviewing & editing.

Data availability Data generated during the current study is provided within the manuscript or supplementary information files. Raw data is available from the corresponding author on request.

Declarations

Competing interests The authors declare no competing interests.

References

1. Amer AA, El-Didamony H, El-Sokkary TM, Wahdan MI. Synthesis and characterization of some calcium aluminate phases from nano-size starting materials. Bol Soc Esp Ceram V. 2022;61:98–106. https://doi.org/10.1016/j.bsecv.2020.07.006.
2. Bayer G, Kahr G, Müller-Vonmoos M. Reactions of ammonium sulphates with kaolinite and other silicate and oxide minerals. Clay Miner. 1982;17:271–83. https://doi.org/10.1180/claymin.1982.017.3.01.
3. Blum AE, Stillings LL. Feldspar dissolution kinetics. In: White AF, Brantley SL, editors. Chemical weathering rates of silicate minerals. Washington, DC: Mineralogical Society of America; 1995. p. 291–351.
4. Borra CR, Mermans J, Blanpain B, Pontikes Y, Binnemans K, Van Gerven T. Selective recovery of rare earths from bauxite residue by combination of sulfation, roasting and leaching. Miner Eng. 2016;92:151–9. https://doi.org/10.1016/j.mineng.2016.03.002.
5. Cagnon B, Daval D, Cabié M, Lemarchand D, Gin S. A comparative study of the dissolution mechanisms of amorphous and crystalline feldspars at acidic pH conditions. npj Mater Degrad. 2022;6:1–13. https://doi.org/10.1038/s41529-022-00240-6.
6. Carincross B. Field guide to rocks and minerals in South Africa. Cape Town: Struik Publishers; 2004.
7. Casey WH, Westrich HR, Holdren GR. Dissolution rates of plagioclase at pH = 2 and 3. Am Mineral. 1991;76:211–7.
8. Castleman BA, van der Merwe EM, Doucet FJ. Thermochemical purification of talc with ammonium sulphate as chemical additive. Miner Eng. 2021;164:1–6. https://doi.org/10.1016/j.mineng.2021.106815.
9. Dietrich RV. Feldspar [www document]. Encycl. Br. https://www.britannica.com/science/feldspar (2018). Accessed 24 Mar 2020
10. Doucet FJ. Scoping study on CO_2 mineralization technologies, contract report no CGS-2011-007. South Africa: South African Centre for Carbon Capture and Storage; 2011.
11. Doucet FJ, Mohamed S, Neyt N, Castleman BA, van der Merwe EM. Thermochemical processing of a South African ultrafine coal fly ash using ammonium sulphate as extracting agent for aluminum extraction. Hydrometallurgy. 2016;166:174–84. https://doi.org/10.1016/j.hydromet.2016.07.017.
12. Eales HV. The bushveld complex: an introduction to the geology and setting of the bushveld complex. Pretoria: Council for Geoscience; 2014.
13. Földvári M. Handbook of thermogravimetric system of minerals and its use in geological practice: occasional papers of the Geological Institute of Hungary, vol. 213. Budapest: Geological Institute of Hungary; 2011.
14. Frankel GS, Vienna JD, Lian J, Guo X, Gin S, Kim SH, Du J, Ryan JV, Wang J, Windl W, Taylor CD, Scully JR. Recent advances in corrosion science applicable to disposal of high-level nuclear waste. Chem Rev. 2021;121:12327–83. https://doi.org/10.1021/acs.chemrev.0c00990.
15. Gin S, Delaye JM, Angeli F, Schuller S. Aqueous alteration of silicate glass: state of knowledge and perspectives. npj Mater Degrad. 2021;5:42. https://doi.org/10.1038/s41529-021-00190-5.
16. Grambow B. Nuclear waste glasses—How durable? Elements. 2006;2:357–64. https://doi.org/10.2113/gselements.2.6.357.
17. Gudbrandsson S, Wolff-Boenisch D, Gislason SR, Oelkers EH. Experimental determination of plagioclase dissolution rates as a function of its composition and pH at 22 °C. Geochim Cosmochim Acta. 2014;139:154–72. https://doi.org/10.1016/j.gca.2014.04.028.
18. Haldar SK, Tišljar J. Chapter 2—basic mineralogy. In: Haldar SK, Tišljar J, editors. Introduction to mineralogy and petrology. Oxford: Elsevier; 2014. p. 39–79.
19. Heřmanská M, Voigt MJ, Marieni C, Declercq J, Oelkers EH. A comprehensive and internally consistent mineral dissolution rate database: part I: primary silicate minerals and glasses. Chem Geol. 2022;597: 120807. https://doi.org/10.1016/j.chemgeo.2022.120807.
20. Hochella MF, Banfield JF. Chemical weathering of silicates in nature: a microscopic perspective with theoretical considerations. In: White AF, Brantley S, editors. Chemical weathering rates of silicate minerals. Chelsea: Mineralogical Society of America; 1995. p. 353–406.
21. Howie RA, Zussman J, Deer W. An introduction to the rock-forming minerals. 2nd ed. England: Pearson Education Limited; 1992.
22. Jeelani PG, Mulay P, Venkat R, Ramalingam C. Multifaceted application of silica nanoparticles—a review. SILICON. 2020;12:1337–54. https://doi.org/10.1007/s12633-019-00229-y.
23. Klein C, Dutrow B, Dana JD, Klein C. Manual of mineral science. New York: Wiley; 2008.
24. Košek F, Culka A, Jehlička J. Raman spectroscopic study of six synthetic anhydrous sulfates relevant to the mineralogy of fumaroles. J Raman Spectrosc. 2018;49:1205–16. https://doi.org/10.1002/jrs.5363.
25. Li J, Li D, Xu Z, Liao C, Liu Y, Zhong B. Selective leaching of valuable metals from laterite nickel ore with ammonium chloride-hydrochloric acid solution. J Clean Prod. 2018;179:24–30.
26. Martins R. Discover materials: the pathway to explore materials as activators of the challenges of the future. Discov Mater. 2021;1:1. https://doi.org/10.1007/s43939-020-00002-8.
27. Meyer NA. An investigation into the dissolution of pyroxene: a precursor to mineral carbonation of PGM tailings in South Africa. MSc thesis, University of Cape Town, South Africa, 2014.
28. Meyer NA, Vögeli JU, Becker M, Broadhurst JL, Reid DL, Franzidis JP. Mineral carbonation of PGM mine tailings for CO_2 storage in South Africa: a case study. Miner Eng. 2014;59:45–51. https://doi.org/10.1016/j.mineng.2013.10.014.
29. Miura H, SuzakiKikuchi HT. Synthesis and properties of the system $Al_2(SO_4)_3$–$Fe_2(SO_4)_3$. Mineral J. 1994;17:42–5.
30. Miura H, Niida K, Hirama T. Mikasaite, $(Fe^{3+}, Al)_2(SO_4)_3$, a new ferric sulphate mineral from Mikasa city, Hokkaido, Japan. Mineral Mag. 1994;58:649–53. https://doi.org/10.1180/minmag.1994.058.393.15.
31. Mohale S, Masetlana TR, Bonga M, Ikaneng M, Dlambulo N, Malebo L, Mwape P. South Africa's mining industry 2013–2014. South Africa: Department of Mineral Resources; 2015. p. 276.
32. Mohamed S. Extraction of major elements from PGE tailings in view of nanoparticle synthesis for environmental technological application. MSc thesis, University of Pretoria, South Africa, 2015.
33. Mohamed S, Lehong K, van der Merwe EM, Altermann W, Doucet FJ. Thermochemical treatment of platinum group metal tailings with ammonium salts for major element recovery. J Therm Anal Calorim. 2019;138:2015–33. https://doi.org/10.1007/s10973-019-08233-5.
34. Mohamed S, van der Merwe EM, Altermann W, Doucet FJ. Addendum to "Process development for elemental recovery from PGM tailings by thermochemical treatment: preliminary major element extraction studies using ammonium sulphate as extracting agent" [Waste Manage 50 (2016) 334–345]. Waste Manag. 2017;66:222–4. https://doi.org/10.1016/j.wasman.2017.04.009.

35. Mohamed S, van der Merwe EM, Altermann W, Doucet FJ. Process development for elemental recovery from PGM tailings by thermochemical treatment: preliminary major element extraction studies using ammonium sulphate as extracting agent. Waste Manag. 2016;50:334–45. https://doi.org/10.1016/j.wasman.2016.02.021.
36. Nduagu E, Björklöf T, Fagerlund J, Wärnå J, Geerlings H, Zevenhoven R. Production of magnesium hydroxide from magnesium silicate for the purpose of CO_2 mineralization—part 1: application to finnish serpentinite. Miner Eng. 2012;30:75–86. https://doi.org/10.1016/j.mineng.2011.12.004.
37. Nduagu EI, Highfield J, Chen J, Zevenhoven R. Mechanisms of serpentine-ammonium sulfate reactions: toward higher efficiencies in flux recovery and Mg extraction for CO_2 mineral sequestration. RSC Adv. 2014;4:64494–505. https://doi.org/10.1039/c4ra08925a.
38. Nkosi ZH. Experimental investigation of the CO_2 storage potential of major Mg and Ca-rich minerals in platinum mine tailings—eastern Bushveld Igneous Complex, South Africa. MSc thesis, University of Pretoria, South Africa, 2017.
39. Oelkers EH, Schott J. The dependence of silicate dissolution rates on their structure and composition. In: Water-rock interaction. Oxfordshire: Routledge; 2021. p. 153–6.
40. Oelkers EH, Schott J. An experimental study of enstatite dissolution rates as funcion of pH, temperature, and aqueous Mg and Si concentration, and the mechanism of pyroxene/pyroxenoid dissolution. Geochim Cosmochim Acta. 2001;65:1219–31. https://doi.org/10.1016/S0016-7037(00)00564-0.
41. Parafiniuk J, Siuda R. High temperature sulfate minerals forming on the burning coal dumps from upper silesia. Poland: Minerals; 2021. https://doi.org/10.3390/min11020228.
42. Seyama H, Kinoshita K, Soma M. Surface alteration of plagioclase during acid dissolution. Surf Interface Anal. 2002;34:289–92.
43. Skoog DA, Holler FJ, Crouch S. Fundamentals of analytical chemistry. 8th ed. Chennai: Cengage Learning; 2004.
44. Tagawa H. Thermal decomposition temperatures of metal sulfates. Thermochim Acta. 1984;80:23–33. https://doi.org/10.1016/0040-6031(84)87181-6.
45. van der Merwe EM, Gray CL, Castleman BA, Mohamed S, Kruger RA, Doucet FJ. Ammonium sulphate and/or ammonium bisulphate as extracting agents for the recovery of aluminum from ultrafine coal fly ash. Hydrometallurgy. 2017;171:185–90. https://doi.org/10.1016/j.hydromet.2017.05.015.
46. van Noort R, Mørkved PT, Dundas SH. Acid neutralization by mining waste dissolution under conditions relevant for agricultural applications. Geoscience. 2018;8:380. https://doi.org/10.3390/geosciences8100380.
47. Vandenberghe RE, de Resende VG, da Costa GM, De Grave E. Study of loss-on-ignition anomalies found in ashes from combustion of iron-rich coal. Fuel. 2010;89:2405–10. https://doi.org/10.1016/j.fuel.2010.01.022.
48. Vogeli J, Reid DL, Becker M, Broadhurst J, Franzidis JP. Investigation of the potential for mineral carbonation of PGM tailings in South Africa. Miner Eng. 2011;24:1348–56. https://doi.org/10.1016/j.mineng.2011.07.005.
49. Wellmann PJ. The search for new materials and the role of novel processing routes. Discov Mater. 2021;1:14. https://doi.org/10.1007/s43939-021-00014-y.
50. Wu T, Chi M, Huang R. Characteristics of CFBC fly ash and properties of cement-based composites with CFBC fly ash and coal-fired fly ash. Constr Build Mater. 2014;66:172–80. https://doi.org/10.1016/j.conbuildmat.2014.05.057.
51. Zhang L, Lüttge A. Theoretical approach to evaluating plagioclase dissolution mechanisms. Geochim Cosmochim Acta. 2009;73:2832–49. https://doi.org/10.1016/j.gca.2009.02.021.